

Comprehensive kinetic study of *Imperata Cylindrica* pyrolysis via Asym2sig deconvolution and combined kinetics

Syarif Hidayat^{a,b}, Muhammad S. Abu Bakar^a, Ashfaq Ahmed^{a,c,d,**}, Dewi Agustina Iryani^e, Murid Hussain^d, Farrukh Jamil^d, Young-Kwon Park^{c,*}

^a Faculty of Integrated Technologies, Universiti Brunei Darussalam, Tungku Link, Gadong, Negara, BE1410, Brunei Darussalam

^b Department of Environmental Engineering, Universitas Banten Jaya, Jl. Ciwaru Raya, Serang, Banten, 42121, Indonesia

^c School of Environmental Engineering, University of Seoul, Seoul, 02504, Republic of Korea

^d Department of Chemical Engineering, COMSATS University Islamabad Lahore Campus, Raiwind Road, Lahore, Punjab, 54000, Pakistan

^e Department of Chemical Engineering, Engineering Faculty, University of Lampung, Jl. Sumantri Brojonegoro 1, Bandar Lampung, 35145, Indonesia

ARTICLE INFO

Keywords:

Pyrolysis kinetics
Pseudo components
Combined kinetic
Deconvolution
Imperata Cylindrica

ABSTRACT

This study examined the non-isothermal kinetics of the slow pyrolysis of *Imperata Cylindrica* (IC). Pyrolysis conditions were developed under the pure N₂ flow and non-isothermal conditions at the heating rates of 2.5, 5, 10, and 17.5 K/min and over the temperature range of 303–1173 K. The IC pyrolysis profiles could be identified into three parallel reactions, each of which corresponded to pseudo-hemicelluloses (P-Hem), pseudo-cellulose (P-Cell), and pseudo-lignin (P-Lig) decomposition. A systematic kinetic study of the pyrolysis of IC via thermogravimetric analysis (TGA) deconvolution using Asymmetric Double Sigmoidal (Asym2sig), Friedman differential iso-conversional and combined kinetics of biomass pseudo-components was carried out. The kinetics parameters of pseudo components fitted well with the pyrolysis experimental data for all the heating rates. Differential master-plots showed that the reaction mechanisms for pseudo hemicellulose (P-Hem) and pseudo cellulose (P-Cell) were diffusional and order based, and high order based (3rd order) for the pseudo lignin (P-Lig). Mechanism of P-Hem, P-Cell and P-Lig could be further reconstructed to Sestak and Berggren model of $f(\alpha) = \alpha^{-0.9875} (1 - \alpha)^{1.325} [-\ln\{\frac{f(\alpha)}{f_0}\}] (1 - \alpha)^{0.0209}$, $f(\alpha) = \alpha^{0.3313} (1 - \alpha)^{1.4731} [-\ln\{\frac{f(\alpha)}{f_0}\}] (1 - \alpha)^{0.0215}$ and $f(\alpha) = \alpha^{-2.9551} (1 - \alpha)^{2.7642} [-\ln\{\frac{f(\alpha)}{f_0}\}] (1 - \alpha)^{0.0074}$, respectively. The combined kinetic reported the activation energies of pseudo-components were as 194.709 kJ/mol, 179.968 kJ/mol and 219.226 kJ/mol for P-Hem, P-Cell and P-Lig, respectively.

1. Introduction

The consumption of non-renewable energy to come upon the growing energy demands has deleterious effects on the environment, such as acidic rain, greenhouse gas emissions, and climate change [1–5]. Furthermore, the reserves of fossil fuel are anticipated to be depleted in the near future. Hence, increasing attention has been paid towards the development and application of cleaner and renewable sources of energy to achieve sustainable future frameworks. Biomass has advantages over other renewable energy resources because it is widely available and carbon-neutral resource. In addition, it can be transformed into biofuel in solid, liquid, and gaseous forms by applying various conversion processes [6–9]. *Imperata cylindrica* (IC) is one of prospective biomass, also

known as cogongrass, alang-alang in Southeast Asia. IC can grow well without any specific nutritional treatments over a wide variety of soil types and is found in various environments, such as grasslands, abandoned fields, highway and railway edges, pine and hardwood jungles, and recreational areas [10].

Among thermochemical technologies, pyrolysis process decompose biomass directly into value-added products in the form of solid (bio-char), liquid (bio-oil), and gaseous biofuels [11–14]. The analysis of the kinetics of the biomass pyrolysis reactions provides fundamental information on how it is decomposed, allowing optimization of the process, and also provides useful data for the reactor design to convert biomass effectively. Kinetics analysis also provides important information on reaction mechanism models to develop mathematical models that

* Corresponding author.

** Corresponding author at: Faculty of Integrated Technologies, Universiti Brunei Darussalam, Tungku Link, Gadong, Negara, BE1410, Brunei Darussalam.

E-mail addresses: drahmed85@uos.ac.kr (A. Ahmed), catalica@uos.ac.kr (Y.-K. Park).

describe the pyrolysis process [15,16].

Kinetic studies on biomass pyrolysis can be estimated in two ways: iso-conversional methods and model-fitting methods [17]. Iso-conversional methods have been developed to examine the kinetic parameters of solid biomass reactions with simple thermal characteristics. In recent studies, the kinetic parameters of biomass included IC were evaluated using these methods [18–21]. On the other hand, the reaction model analysis familiar with a single step method via master-plots owing to homogeneity in the biomass pyrolysis process were evaluated [21].

The data from the single components biomass pyrolysis mechanism cannot describe the thermal behaviour of biomass. This is considered contradictory rather than complementary in the complexity of the reaction kinetics [17,22]. The multi components analysis of biomass pyrolysis provided more detailed knowledge about the simulation and modelling of thermochemical reactions [23]. International Confederation for Thermal Analysis and Calorimetry (ICTAC) [24] recommended comprehensive kinetic analysis to represent the distributed reactivity analysis because biomass components are complex materials, in which the decomposition occurs through multiple, independent and parallel reactions. Oladokun et al. [20] performed model fitting for a kinetic study by the multi-step de-volatilization of IC by assuming the reaction model of pseudo-components as parallel first-order reactions. Furthermore, numerous kinetic studies of biomass decomposition through Distributed Activation Energy Model (DAEM) and nth order-based kinetics have been reported [25,26]. Poletto et al. [27] reported that the first-order or n-order models to analyse the degradation process have an erroneous physical meaning and order because of the combined effects of some mechanisms. In this context, an investigation of comprehensive pyrolysis kinetic analysis via combination deconvolution and combined kinetic would be important. The systematic approaches in multi-step kinetics are thermogravimetric analysis (TGA) deconvolution, iso-conversional method, master plot analysis and combined kinetics. Systematic multi-step kinetics can offer more precise info on the modelling and simulation of pyrolysis reactions [23]. Based on the deconvolution method, the reaction rates are separated into three main components in biomass: pseudo hemicellulose, cellulose, and lignin. The obtained deconvolution profiles of the pseudo-components of biomass can be analysed by the kinetic parameters and reaction model by iso-conversional method, master plot and combined kinetics [24].

In various studies regarding the deconvolution of biomass pyrolysis, thermogram profile was deconvoluted by symmetric functions (Logistic, Gaussian, and Lorentz functions) [28–30] or asymmetric functions (Asymmetric Double Sigmoidal, Weibull, Fraser–Suzuki functions and Bi-Gaussian) [21,30–32]. Among these functions, recent studies [32–34] have shown that Asymmetric Double Sigmoidal (Asym2sig) functions gave an appropriate deconvolution for the kinetic model. To the best of the authors knowledge there are no studies regarding the comprehensive deconvolution and combined kinetic pyrolysis of IC reported yet in literature. Hence, this study to proposed the systematic kinetic pyrolysis of IC via thermogravimetric analysis (TGA) deconvolution using Asym2sig, iso-conversional method, master plot and combined kinetic is the first report of this kind. The systematic multi-step kinetic offer reliable calculation of kinetic parameters and good model description of pyrolysis. Thermogravimetric analysis and differential thermal gravimetric analysis (TGA/DTG) analysis at four different heating rates were carried out. In addition to this, IC biomass was also characterized by the proximate and ultimate analysis, compositional analysis, and Fourier transform infrared (FTIR) to report its bioenergetic value. This study is expected to put forward the beneficial management solution of *Imperata Cylindrica* biomass to produce bio-oil for the energy requirements, which at the present are heavily dependent on the fossil fuels.

Table 1

Physicochemical characteristics of *Imperata Cylindrica* biomass [35].

Proximate Analysis* (wt. %)	
Moisture	6.80
VM	72.01
FC	18.21 ^a
Ash	2.97
Elemental Analysis* (wt. %)	
C	44.38
H	5.65
N	0.82
O	49.06 ^a
S	0.09
O/C**	0.83
H/C**	1.53
Molecular Formula	
CH _{1.528} O _{0.829} N _{0.016}	
Calorific Value* (MJ/kg)	
HHV	18.39
HHV _{correlation}	18.47
Compositional Analysis* (wt. %)	
Hemicellulose	25.13
Cellulose	44.49
Lignin	17.89
Extractives	12.49

HHV_{correlation} = 0.2791 N + 0.3984 C + 0.4030 H - 1.8644 S - 0.03153 O [63].

* Based on dried basis.

** Molar ratio.

^a By difference.

2. Methodology

2.1. Materials

The *Imperata Cylindrica* (IC) biomass was gathered from a grassland in Muara District, Brunei Darussalam. The biomass samples were crushed and sieved to obtain the particles within a size range of 0.125 mm to 0.25 mm, and subsequently dried in a furnace at 50 °C for 24 h to reduce the moisture content.

2.2. Characterization of the feedstock

The biomass of IC was characterized based on proximate and ultimate analyses, compositional analysis, and Fourier-transform infrared (FTIR) analysis by Perkin Elmer Frontier spectroscopy. A detailed description of the ultimate and proximate analysis and compositional analysis are reported elsewhere [35]. FTIR spectroscopy was used to analysis the functional groups of the IC sample. The spectra were generated using a scan range of 600 to 4000 cm⁻¹ with steps of 1 cm⁻¹.

2.3. Thermogravimetric analysis (TGA)

Thermogravimetric analysis (TGA) by Hitachi SII EXSTAR 7300 Series was performed using the parameters for kinetic modelling according to ICTAC recommendation [36]. Approximately 5–10 mg of IC with a range of particle sizes, 0.125 mm – 0.25 mm, were heated at four heating rates of 2.5 K/min, 5 K/min, 10 K/min, and 17.5 K/min, from room temperature to 1173 K under a pure N₂ environment at the flow rate of 100 mL min⁻¹. The thermogram data were analysed using different software, Origin, MATLAB and Microsoft Excel. The Asym2sig deconvolution resulted derivative thermogravimetry (DTG) of

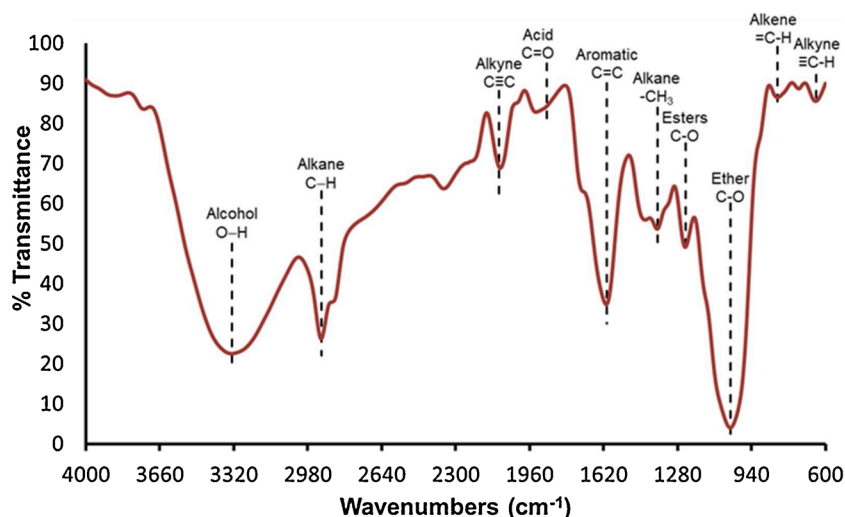


Fig. 1. FTIR spectra of *Imperata Cylindrica*.

Table 2

The functional groups detected in the *Imperata Cylindrica*.

Wavenumbers (cm ⁻¹)	Band position (cm ⁻¹)	Functional group
3200 – 3600	3329	Alcohol
2850 – 3000	2917	Alkane
2100 – 2260	2190	Alkyne
1795 – 1850	1830	Acid
1580 – 1615	1605	Aromatic
1350 – 1480	1373	Alkane
1180 – 1260	1243	Phenolic
1020 – 1120	1037	Ether
675 – 1000	819	Alkene
600 – 700	643	Alkyne

pseudo-hemicellulose (P-Hem), pseudo-celluloses (P-Cell) and pseudo-lignin (P-Lig). To identify the main component of IC sample based on order of peak temperature (T_p), where $T_p(\text{P-Hem}) < T_p(\text{P-Cell}) < T_p(\text{P-Lig})$. In addition to the peak width (W_p) of $W_p(\text{P-Lig}) > W_p(\text{P-Hem}) > W_p(\text{P-Cell})$ [32].

3. Theoretical background of the study

Theoretical background of the study is provided in the supplementary data.

4. Results and discussions

4.1. Physicochemical characteristics

Table 1 lists the physicochemical properties of IC biomass used in this study. IC had a low moisture (6.80 %) content, ash (2.97 %) content, and a high value of (72.01%) volatile matter. The ultimate analysis results reported that the mass percentage of carbon (C), hydrogen (H), nitrogen (N), oxygen (O), and sulphur were 44.38 %, 5.65 %, 0.82 %, 49.06 %, and 0.09 %, respectively. Ultimate analysis showed that the molecular formula of the organic composition of IC was $\text{CH}_{1.528}\text{O}_{0.829}\text{N}_{0.016}$. The high content of volatile matter in addition to low nitrogen and sulphur designate IC as a valued candidate for pyrolysis to bio-oil from environmental emissions perspectives [37]. These properties have similarity to established bioenergy crops, such as *Miscanthus giganteus* (volatile = 72.5 %, N = 1.21 % and S = 0.1 %) [38], *Acacia auriculiformis* [39], rice husk [40] and sugarcane bagasse (volatile = 71.79 %, N = 0.26 % and S = 0.06 %) [41]. The calorific value (HHV) acquired from the analysis (HHV = 18.39 MJ/kg) has a comparable value to the calorific value from calculations (HHV = 18.47 MJ/kg).

The calorific value (HHV) on a dry basis shows that the calorific value of IC is higher than *Miscanthus giganteus* (HHV = 16.58 MJ/kg) [38] and sugarcane bagasse (HHV = 17.24 MJ/kg) [41]. Huang et al. reported that the calorific value HHV increases with increasing C and H

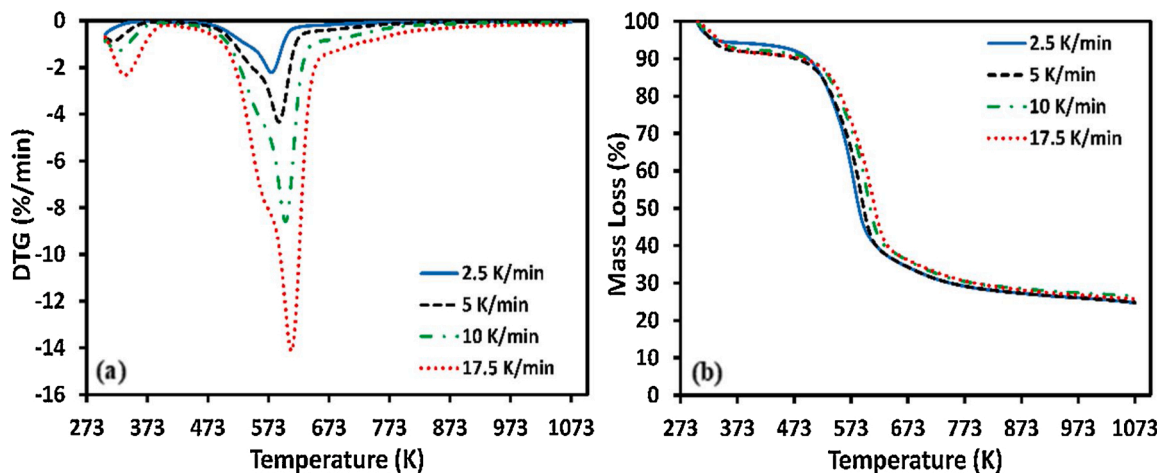
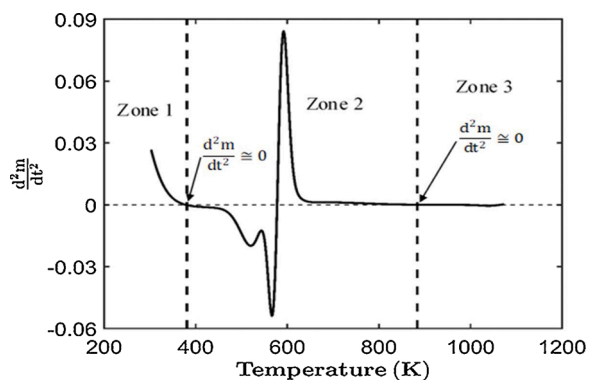


Fig. 2. DTG (a) and TGA (b) curves in N_2 atmosphere at four heating rates.

Table 3

Characteristic temperatures of the different zones during pyrolysis process.

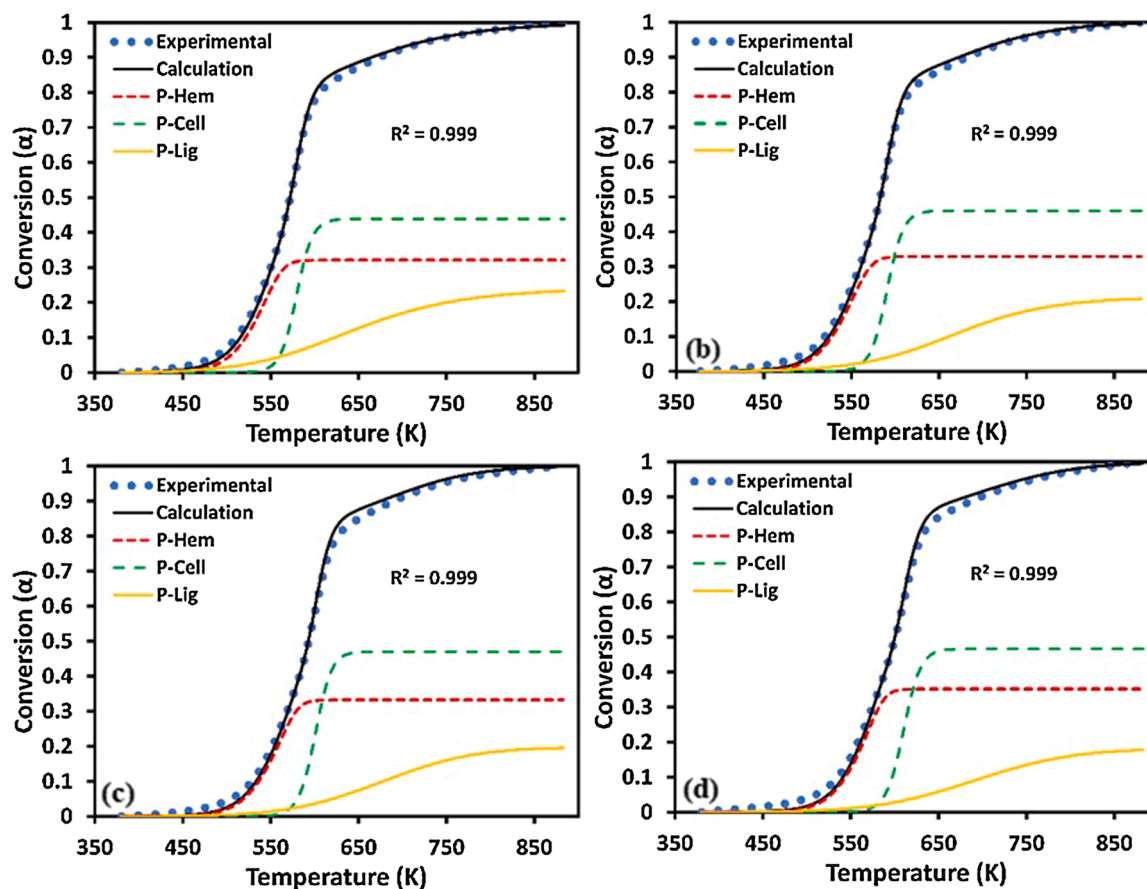
Heating Rate (K/min)	Zone 1		Zone 2			Zone 3	
	T _i (K)	T _f (K)	T _i (K)	T _p (K)	T _f (K)	T _i (K)	T _f (K)
2.5	303.04	380.64	380.64	578.53	883.84	883.84	1072.98
5	303.41	380.49	380.49	590.38	883.19	883.19	1073.00
10	303.58	380.33	380.33	601.20	882.65	882.65	1072.98
17.5	303.71	380.06	380.06	610.79	882.60	882.60	1072.88

**Fig. 3.** Characteristic of pyrolysis zone by using derivative DTG.

content but alleviate with increasing N content [42]. Compositional analysis (Table 1) of IC revealed 25.13 % hemicelluloses, 12.49 % extractive, 17.89 % lignin, and 44.49 % cellulose. IC has a lower lignin

content than *Mischantus giganteus* (23.4 %) [43] and sugarcane bagasse (19.2 %) [44]. The variation of the chemical compositions of bio-oil in the literature can be explained by the different results of compositional analysis of IC and bioenergy crops.

The FTIR was performed to analyze the functional groups in the IC biomass. Fig. 1 presents the FTIR spectra, and Table 2 lists the corresponding wavenumber and atomic bonds of the functional groups. The broad absorption for IC at 3329 cm^{-1} $200\text{--}3600\text{ cm}^{-1}$ was intended to the O–H stretching vibration, indicating phenolic and/or alcohol groups [45]. The peaks at 2916 cm^{-1} and 2190 cm^{-1} were assigned C–H and C≡C stretching vibrations. The presence of a C=O stretching vibration at 1830 cm^{-1} confirmed the existence of ketones, esters, aldehydes, and carboxylic acid [46]. The absorbance at 1580 to 1615 cm^{-1} was presented to C=C stretching vibrations associated with aromatics or alkenes. Ether substitutions could be found from the area =C–H warping vibrations at 819 cm^{-1} [47]. At high intensity, the wavelength range, $1020\text{--}1120\text{ cm}^{-1}$ caused by C–O tensing vibrations, resembles to the primary, secondary, and tertiary alcohols, and ether [48]. The low-intensity peak at $600\text{--}700\text{ cm}^{-1}$ was assigned to ≡C–H originating from phenyl ring substitution and alkynes bends [49].

**Fig. 4.** Deconvolution of TGA profile of IC at four heating rates (a). 2.5 K/min, (b). 5 K/min, (c). 10 K/min, and (d). 17.5 K/min.

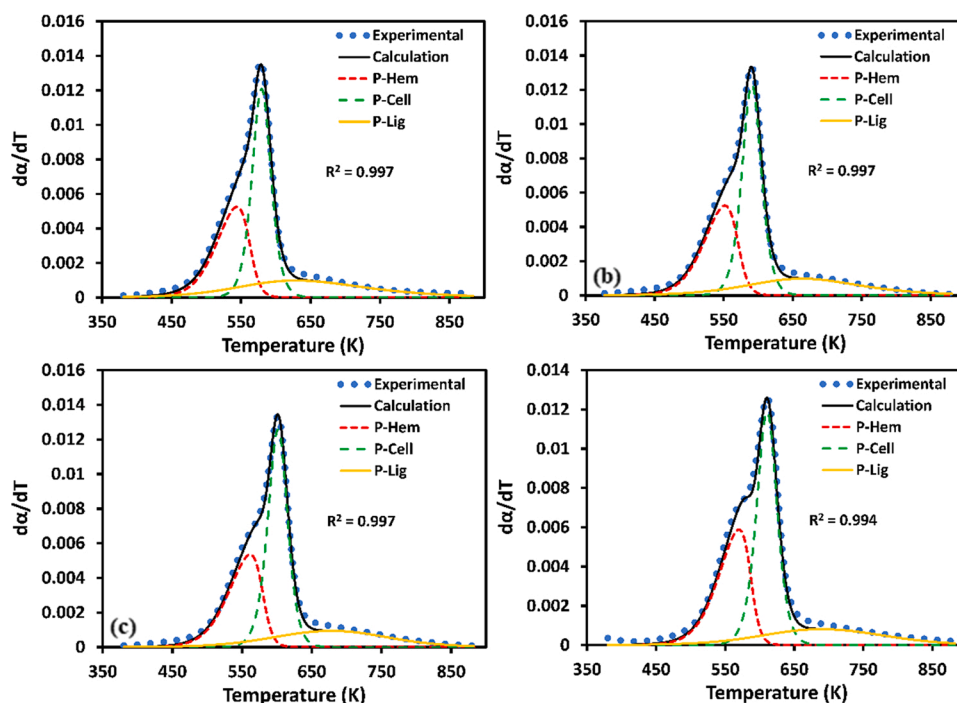


Fig. 5. Deconvolution of DTG profile of IC at four heating rates (a). 2.5 K/min, (b). 5 K/min, (c). 10 K/min, and (d). 17.5 K/min.

4.2. Thermal behaviour

Fig. 2 (a–b) presents the DTG/TGA plots of the thermal behaviour of IC under the N_2 atmosphere at various heating rates. The heating rate influenced the pyrolysis process of IC. The thermal degradation characteristics showed that the rate of mass-loss and peak temperature switched to a high temperature when the heating rate was raised from 2.5–17.5 K/min which suggested that at a lower heating rate, biomass particle heating occurs more gradually, which results in a longer heating time. As a result, the conversion rate was slow at the low heating rates, and the decomposition temperature was higher in a short time of thermal shock. The pyrolysis of IC can be divided into three zones of the DTG profiles. Based on derivative DTG, the preliminary (T_i) and final temperature (T_f) of each zone can be determined, as shown in Table 3 and Fig. 3. The first zone from ambient temperature to approximately 380 K was associated with the initial loss of mass biomass due to moisture removal. The second zone, ranging from approximately 380 K–883 K, was the major pyrolysis stage due to devolatilization. In this zone, one peak and one shoulder, as well as one long tail, could be considered for the degradation of three major components of biomass. The shoulder signifies the fastest degradation of hemicellulose. The peak was attributed to the conversion of cellulose component, and the tailing was associated mainly with the devolatilization of lignin. The third zone ranging from 883 K–1073 K, showed a very small loss of mass due probably to the carbonaceous degradation of residues.

4.3. DTG/TGA curve deconvolution

The DTG and TGA curves were deconvoluted to each pseudo-component using the Asym2sig function. In this work, the Asym2sig function Eq. (S2 – S6) was applied to deconvolute the rate ($d\alpha/dT$) and the conversion value using the integral deconvolution in zone 2 of the TGA/DTG data. Figs. 4 and 5 present the deconvolution profile of TGA and DTG at several heating rates (2.5, 5, 10, and 17.5 K/min). Three deconvolution profiles at four different heating rates were observed, which were associated with the pyrolysis of pseudo-hemicellulose (P-Hem), pseudo-cellulose (P-Cell), and pseudo-lignin (P-Lig). The three peaks increased with increasing heating rate. Moreover, the

deconvolution (Figs. 4 and 5) data can be applied to calculate ($d\alpha/dT$) and the conversion (α) profile for pseudo-components at all heating rates. Fig. 6 shows the ($d\alpha/dT$) and conversion (α) profile of P-Cell (Fig. 6 a,b), P-Hem (Fig. 6 c,d), and P-Lig (Fig. 6 e,f). Table 4 lists the Asym2sig parameters and the contributing factor of the pseudo-components.

4.4. Friedman differential iso-conversional

The deconvolution of TGA/DTG in previous section had generated the data percentage conversion and conversion rate of the respective pseudo components biomass at four heating rates. The activation energy of each biomass constituents could be further estimated using Friedman iso-conversional method.

The Friedmann plots for the pyrolysis of individual constituent's IC biomass are presented in Fig. 7 (a – c) and the average activation energies (E_a) for components showed in Table 5. It can be exhibited that under certain conversion (α) gave good degree of linear relationship between $\ln \left[\beta \frac{d\alpha}{dT} \right]$ vs $\frac{1}{T}$ in Eq. (S9) for P-Hem, P-Cell and P-Lig. In this study, the conversion ranges was selected from 0.05 to 0.95 with step size 0.05, as recommended by ICTAC [17]. For all biomass constituents, in the conversion range of 0.05 – 0.95, E_a increases with the conversion (α) increasing. The E_a varied in the range of 158.496–247.883 kJ.mol⁻¹, 175.221–193.091 kJ.mol⁻¹ and 75.898–503.222 kJ.mol⁻¹ for P-Hem, P-Cell and P-Lig, respectively. The activation energy ranges of P-Lig provided quite broad range (75.898–503.222 kJ.mol⁻¹) compare to P-Cell and P-Hem. Anca-Couce, et al., [50] reported that the values of the activation energy of P-Lig pyrolysis vary greatly and covers a wider temperature from low temperature with very low activation energy to high temperature with high activation energy. Furthermore, P-Lig as an amorphous three-dimensional polymer with strong linkage and higher thermal stability caused the reaction rate of lignin is slow and occurs over the entire pyrolysis temperature interval [51]. Moreover, the value of activation energy average (E_{av}) for P-Hem, P-Cell and P-Lig were 198.117 kJ.mol⁻¹, 181.135 kJ.mol⁻¹ dan 190.766 kJ.mol⁻¹, respectively. Further, the results show the variation of activation energy as can

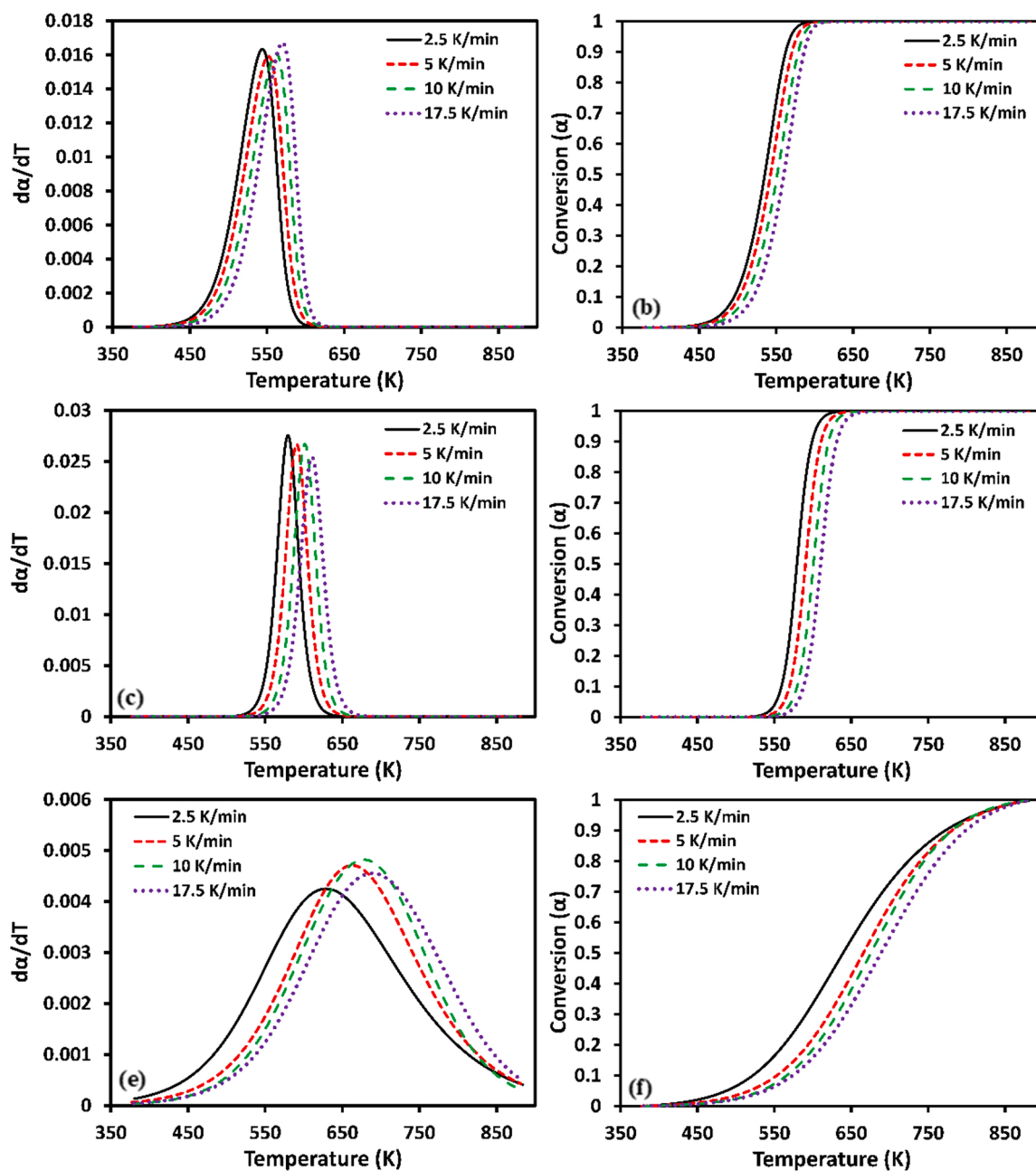


Fig. 6. Profile ($d\alpha/dT$) and (α) of P-Hem (a,b), P-Cell (c,d), and P-Lig (e, f).

Table 4
Asym2sig parameters and contribution factor of P-Hem, P-Cell and P-Lig.

Heating Rate (K/min)	Pseudo Components	c_i	$x_{p,i}$	A_i	$w_{1,i}$	$w_{2,i}$	$w_{3,i}$
2.5	P-Hem	0.321	540.778	0.023	41.418	18.670	7.384
	P-Cell	0.439	579.982	0.099	2.046	9.317	8.823
	P-Lig	0.232	616.154	0.010	65.691	47.165	73.845
5	P-Hem	0.329	548.412	0.022	42.586	19.128	7.587
	P-Cell	0.460	591.319	0.090	3.223	9.677	9.016
	P-Lig	0.208	646.834	0.021	-15.532	47.987	62.470
10	P-Hem	0.333	557.441	0.022	42.886	19.420	6.932
	P-Cell	0.471	602.381	0.070	8.642	9.955	8.479
	P-Lig	0.196	666.215	0.167	-139.984	42.359	45.568
17.5	P-Hem	0.352	565.992	0.023	40.933	18.892	6.608
	P-Cell	0.466	611.420	0.074	6.620	10.294	9.195
	P-Lig	0.178	704.618	0.183	-155.326	48.221	44.263

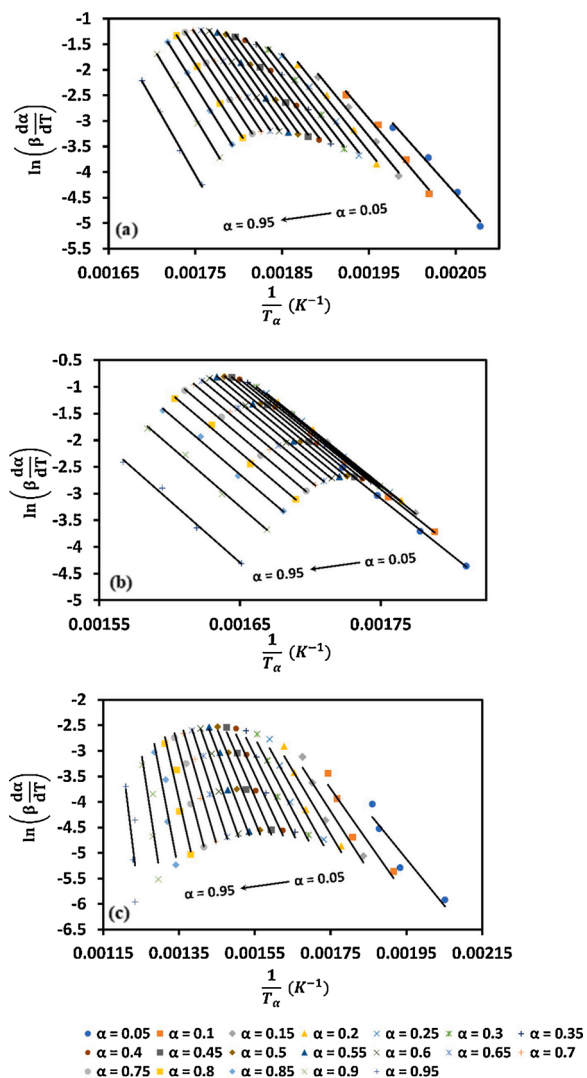


Fig. 7. Friedmann Iso-conversional Plots for P-Hem (a), P-Cell (b) and P-Lig (c).

Table 5

Results of the activation energies (E_{α}) and factor correlation coefficients (R^2).

α	P-Hem		P-Cell		P-Lig	
	E_{α} (kJ/mol)	R^2	E_{α} (kJ/mol)	R^2	E_{α} (kJ/mol)	R^2
0.05	158.496	0.984	175.221	1.000	75.898	0.908
0.10	167.244	0.989	175.616	1.000	87.674	0.914
0.15	172.836	0.992	176.017	1.000	96.355	0.919
0.20	177.155	0.993	176.440	1.000	103.859	0.926
0.25	180.804	0.995	176.894	0.999	110.929	0.933
0.30	184.063	0.996	177.386	0.999	117.975	0.941
0.35	187.092	0.997	177.920	0.999	125.288	0.948
0.40	190.001	0.997	178.502	0.999	133.121	0.956
0.45	192.878	0.998	179.137	0.999	141.734	0.962
0.50	195.798	0.998	179.829	0.999	151.433	0.967
0.55	198.837	0.999	180.588	0.999	162.608	0.971
0.60	202.079	0.999	181.421	0.998	175.794	0.973
0.65	205.616	0.999	182.345	0.998	191.769	0.972
0.70	209.565	1.000	183.377	0.998	211.728	0.967
0.75	214.081	1.000	184.550	0.997	237.621	0.957
0.80	219.396	1.000	185.915	0.996	272.840	0.935
0.85	225.910	1.000	187.571	0.995	323.641	0.891
0.90	234.489	0.999	189.735	0.994	401.071	0.792
0.95	247.883	0.997	193.091	0.991	503.222	0.521
Average	198.117	0.996	181.135	0.998	190.766	0.913

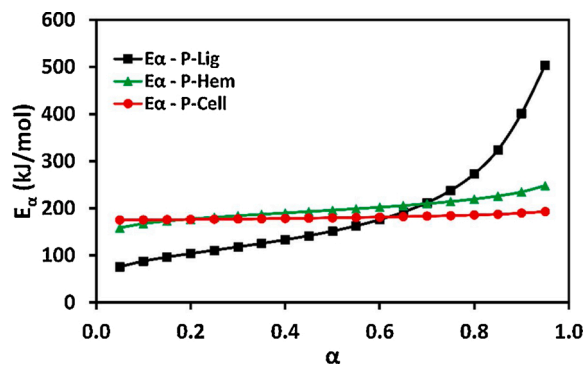


Fig. 8. Variation activation energies of P-Hem, P-Cell and P-Lig via Friedman method.

Table 6

Percentage of E_{α} minimum and E_{α} maximum deviation.

Pseudo - components of Biomass	Minimum E_{α} (kJ/mol)	Maximum E_{α} (kJ/mol)	$E_{\alpha v}$ (kJ/mol)	% E_{α} Min Deviation	% E_{α} Max Deviation
P-Hem	158.496	247.883	198.117	20.00%	25.12 %
P-Cell	175.221	193.091	181.135	3.26%	6.60 %
P-Lig	75.898	503.222	190.766	60.21%	163.79 %

be seen in Fig. 8 and Table 6, the E_{α} variation of P-Cell lower compared to P-Hem and P-Lig. As can be seen in Table 6, the high dependency E_{α} vs α for P-Hem and P-Lig higher than 20 %. As stated by Vyazovkin et al. [17], when the percentage deviation E_{α} more than 20 % percent to $E_{\alpha v}$ between E_{α} minimum or maximum values, signify the pyrolysis processes of P-Hem and P-Cell or overall pyrolysis of IC was multiple reaction mechanism. Hence, in order to obtain reliable kinetic estimation, combined kinetic analysis would be applied.

4.5. Analysis of reaction mechanism

The differential master plots method was used to estimate the reaction mechanism involved during the thermal decomposition of each pseudo-components. By using the $E_{\alpha v}$ and T_{α} values from Friedman iso-conversional method, $\gamma(\alpha)$ vs. α profiles for three main IC biomass constituents were as shown in Fig. 9. The appropriate reaction mechanisms were determined by comparing the experimental and theoretical curves. It was observed that pyrolysis of P-Hem (Fig. 9a) follows diffusional reaction mechanism (D2, D3 and D4) in the range $0.05 < \alpha < 0.95$ and 2nd order (F2) in the range $0.5 < \alpha < 0.95$ based. Furthermore, belong to pyrolysis of P-Cell (Fig. 9b) in the $0.5 < \alpha < 0.95$ range, the $\gamma(\alpha)$ vs. α profiles have the shape diffusional reaction mechanism (D2, D3 and D4) and 1st order (F1) in the range $0.25 < \alpha < 0.95$. The P-Lig pyrolysis mechanism showed high-order model (3rd order, F3) in the range $0.5 < \alpha < 0.95$ and α below 0.5 present no exact reaction model as per listed in the Table. S1. This could be explained to the structure complexity of P-Lig. Basically, the natural polymer of lignin structure is an amorphous three-dimensional structure that have a phenylpropane structure. Furthermore, the results of the comparison ideal reaction mechanism as showed in the Fig. 9a, c and e could be applied as reference to determine empirical reaction model of Sestak and Berggren.

4.6. Mechanism reconstruction of Sestak and Berggren empirical model

The optimisation of Sestak and Berggren (SB) model in Eq. (S13) was performed based on excel solver. The maximum and minimum range for m, n and p of respective pseudo-components based on a previously study [51]. To perform a best fitting result, the estimation ranges and initial guess of m, n, and p are required. Where the n is belonging to nth order

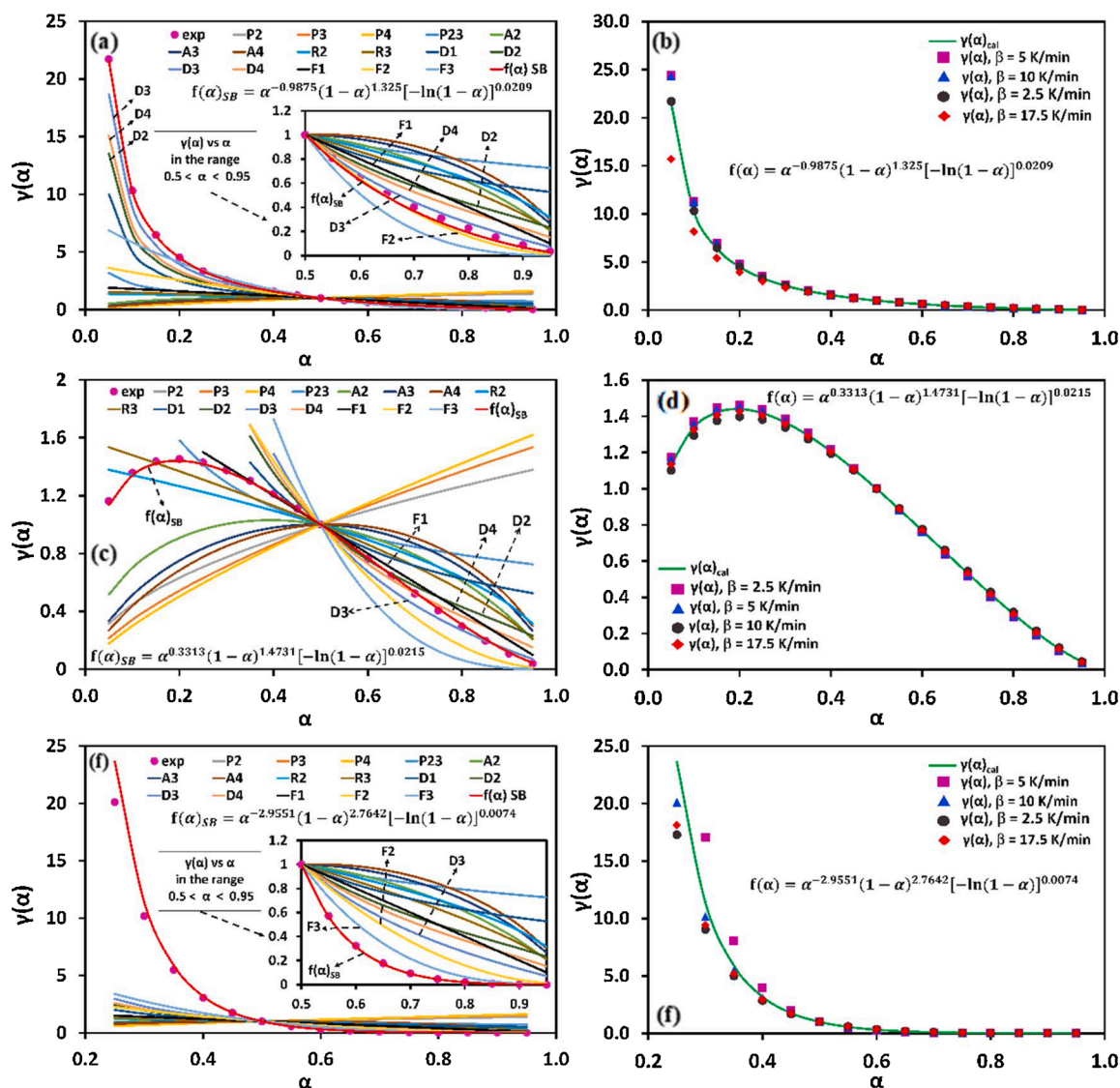


Fig. 9. Differential master Plots dan reconstructed Sestak-Berggren reaction mechanism for P-Hem (a-b), P-Cell (c-d) and P-Lig (e-f) of IC.

Table 7

Correlation coefficient of $\gamma(\alpha)_{exp}$ vs $\gamma(\alpha)_{cal}$ of sestak and berggren empirical model.

Heating Rate (K/min)	Correlation Coefficient (R^2)		
	P-Hem	P-Cell	P-Lig
2.5	0.984	0.999	0.824
5	0.985	0.999	0.967
10	1.000	0.997	0.854
17.5	0.848	1.000	0.901

reaction mechanism and range for n was $0 < n < 7$. The m denotes to Power law model which have range value of m was $-8 < m < 8$. Furthermore, The term of $[-\ln(1-\alpha)]^p$ show the Nucleation reaction model with $-8 < p < 8$ range value of p . The initial guess value of m , n , and p of each pseudo components based on analysis in the Section 4.5. Reaction model of P-Hem follow D2 and F2 (initial guess: $m = 0$, $n = 2$ and $p = -1$). The initial guess $m = 0$, $n = 1$ and $p = -1$ (D2 and F1 reaction mechanism) belong to P-Cell. Moreover, the initial guess for P-Lig follow 3rd order ($m = 0$, $n = 3$ and $p = 0$).

Fig. 9b, d and f shows the fitting results of model via Sestak and Berggren empirical model (SB model). The best model for P-Hem, P-Cell and P-Lig were $f(\alpha) = \alpha^{-0.9875}(1-\alpha)^{1.325}[-\ln(1-\alpha)]^{0.0209}$, $f(\alpha) = \alpha^{0.3313}(1-\alpha)^{1.4731}[-\ln(1-\alpha)]^{0.0215}$ and $f(\alpha) = \alpha^{-2.9551}(1-\alpha)^{2.7642}[-\ln(1-\alpha)]^{0.0074}$, respectively. As can be seen from Fig. 9 and Table 7, R^2 correlation was more than 0.8 for all pseudo components at four heating rates, which mean that the SB model predicted the pyrolysis model of P-Hem, P-Cell and P-Lig very well. As per the theoretical reaction mechanism, $m = -0.9875$ for P-Hem and $m = -2.9951$ for P-Lig signify that there was contribution from the 2/3-Power law (P23) and 1-D diffusion (D1) model. The value $m = 0.3313$ for P-Cell denote caused by power law (P2, P3 and P4) mechanism. The optimum parameters values of n were higher than 1st order model reaction ($n = 1$) for all pseudo components, which indicate that there are Geometrical contraction, Order based, and Diffusion model contribution.

The results of p value were slightly lower for all pseudo components ($0.007 < p < 0.02$), which indicate that the pyrolysis of P-Hem, P-Cell and P-Lig from IC was low contribution from Nucleation mechanism. These results were in line with the results from Section 4.5 that

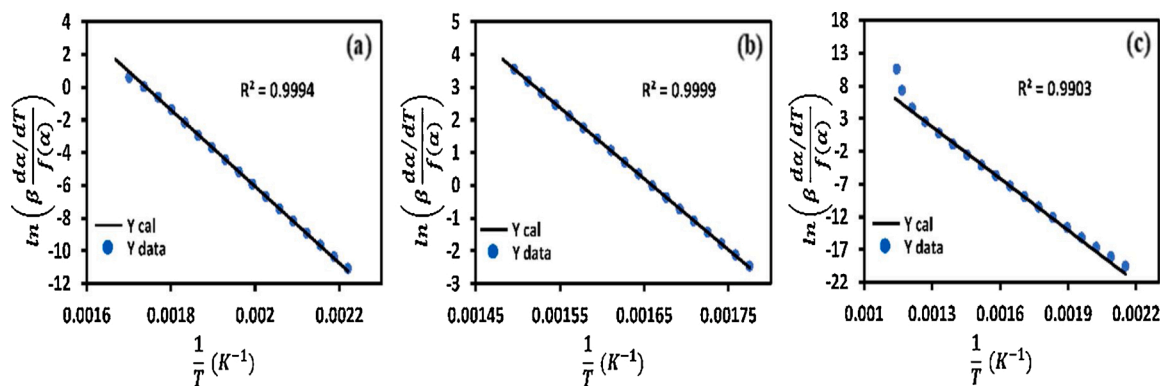


Fig. 10. Combined kinetics analysis of IC pyrolysis: (a) P-Hem, (b) P-Cell and (c) P-Lig.

Table 8

Result parameters, pre-exponential factors, activation energy, and factor correlation (R^2) obtained by CK.

Components	m	n	p	E (kJ/mol)	lnA (ln min ⁻¹)	Correlation Coefficient (R^2)
P-Hem	-0.9875	1.3250	0.0209	194.709	40.774	0.9994
P-Cell	0.3313	1.4731	0.0215	179.968	35.985	0.9999
P-Lig	-2.9551	2.7642	0.0074	219.226	36.048	0.9903

Nucleation model gave poor contribution.

4.7. Combined kinetic (CK) of pseudo components

CK could be used to define the pre-exponential factor (A) and activation energy (E) from the linearisation in Eq. (S14) after determining the reaction mechanism models ($f(\alpha)$). The best fit of reaction models in

the Section 4.6 would be applied to estimate values of kinetic parameters each of pseudo components and using single heating ($\beta = 5$ K/min). Owing to the low accuracy in a single heating rate, the obtained kinetic parameters of the CK technique could be applied to all the observed heating rates according to the suggestion by ICTAC [17]. Fig. 10(a-c) and Table 8 present the linear fitting results of CK and the correlation coefficients (R^2) were high, where $R^2 > 0.99$ for all pseudo components.

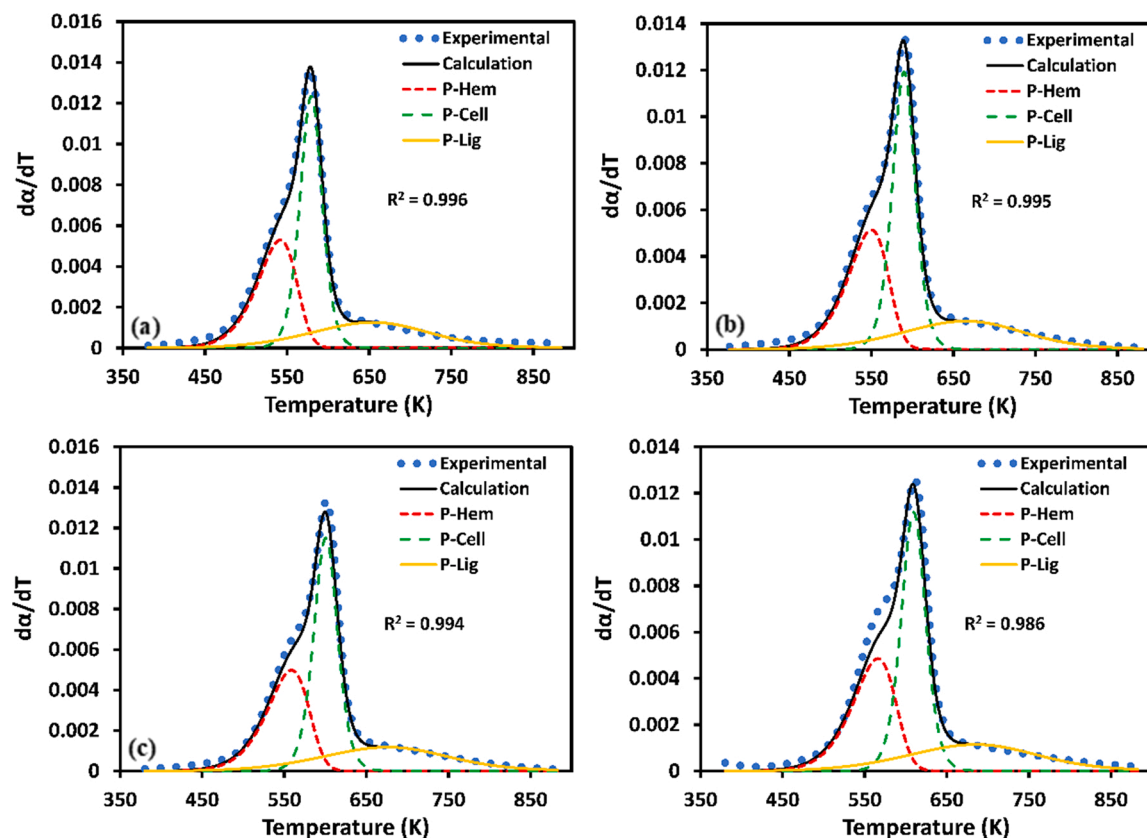


Fig. 11. DTG profiles comparison experimental and calculation CK of *Imperata Cylindrica* pyrolysis at four heating rates (a). 2.5 K/min, (b). 5 K/min, (c). 10 K/min, and (d). 17.5 K/min.

The activation energy of P-Lig (219.226 kJ/mol) pyrolysis was the highest one, followed in order by P-Hem (194.709 kJ/mol) and P-Cell (179.968 kJ/mol). The percentages of deviation activation energy between CK to Friedman method were 1.7 %, 0.6 % and 14.9 % for P-Hem, P-Cell and P-Lig, respectively. The deviation of activation energy results for all of components follow the recommendation below of upper limit 20 % for linear regression method [51,52]. In previous studied by O. Oladokun [20] had been obtained $E_{\text{Hemicellulose}} = 12.94$ kJ/mol, $E_{\text{Cellulose}} = 14.26$ kJ/mol and $E_{\text{Lignin}} = 12.66$ kJ/mol that significantly lower than in this study and literatures [50,53,54]. The result in this study performed the activation energy hemicellulose higher than cellulose, whereas some literatures reported the activation energy of hemicellulose lower than cellulose [50,53]. Furthermore within the study reported by Subramanian et al. [55] ($E_{\text{Hemicellulose}} = 229.0$ kJ/mol) and Siddiqi et al. [56] ($E_{\text{Hemicellulose}} = 191.90$ kJ/mol) have obtained the value of activation energy of hemicellulose and order value activation energy of hemicellulose higher than cellulose, which are similar to this study. As reported in the study Siddiqi et al. [56], high activation energy of hemicellulose could be caused by the structural heterogeneity, synergetic and the catalysing effect of neighbouring -OH groups and metals in the ash. Meanwhile Dussan et al. [57] and Moriana et al. [58] explained that the high activation energy of hemicellulose probably correspond to softwood and grasses that have content of glucomannan upto around 5–20 % of hemicellulose structure, its properties show thermally resistant and higher thermal-stability values. Furthermore, Moriana et al. [58] performed that glucomannan have high activation energy of around 218–230 kJ/mol.

The value of $E_{\text{P-Cell}}$ (179.968 kJ/mol) was comparable with other literatures 175.6 kJ/mol [59], 186.5 kJ/mol [15], 179.54 [25], and 179.87 [60]. As indicated effect of structural heterogeneity, synergetic

and the catalysing effect, hence the value of $E_{\text{P-Cell}}$ lower than value of $E_{\text{P-Hem}}$ and $E_{\text{P-Lig}}$. Furthermore, the activation energy of P-Lig exhibited higher than P-Hem and P-Cell, indicate that lignin as an amorphous three-dimensional polymer, consists of three major basic units: p-coumaryl, coniferyl, and sinapyl, which are linked by ether bonds, ester bonds, and carbon-carbon bonds. Ether bonds present as a phenylpropane side chain, and a benzene ring is the most dominant in lignin, accounted for around 70 % of the total linkages. This linkage ring of lignin is strong and causes higher thermal stability than cellulose and hemicellulose. Therefore, the reaction rate of lignin is slow and occurs over the entire pyrolysis temperature interval; it is completed at below 800 °C [61]. The first stage of lignin decomposition is within the interval of 150 °C–400 °C. The main ether linkages are broken down and converted to o-vanillin, guaiacol, and o-quinone methide. When the temperature of lignin pyrolysis continued to increase after 400 °C, the benzene rings were destroyed and transformed into non-condensable gases [62].

The $\ln A$ values of respective P-Hem, P-Cell and P-Lig was 40.774 $\ln \text{m}^{-1}$ ($A = 5.103 \times 10^{17} \text{ m}^{-1}$), 35.985 $\ln \text{m}^{-1}$ ($A = 4.246 \times 10^{15} \text{ m}^{-1}$) and 36.048 $\ln \text{m}^{-1}$ ($A = 4.524 \times 10^{15} \text{ m}^{-1}$). The pyrolysis kinetics equation of respective pseudo components IC based on CK can be written as:

For P-Hem:

$$\frac{d\alpha_H}{dT} = \frac{5.103 \times 10^{17}}{\beta} \exp\left(\frac{-194709}{RT}\right) \alpha_H^{-0.9875} (1 - \alpha_H)^{1.325} [-\ln(1 - \alpha_H)]^{0.0209} \quad (1)$$

For P-Cell:

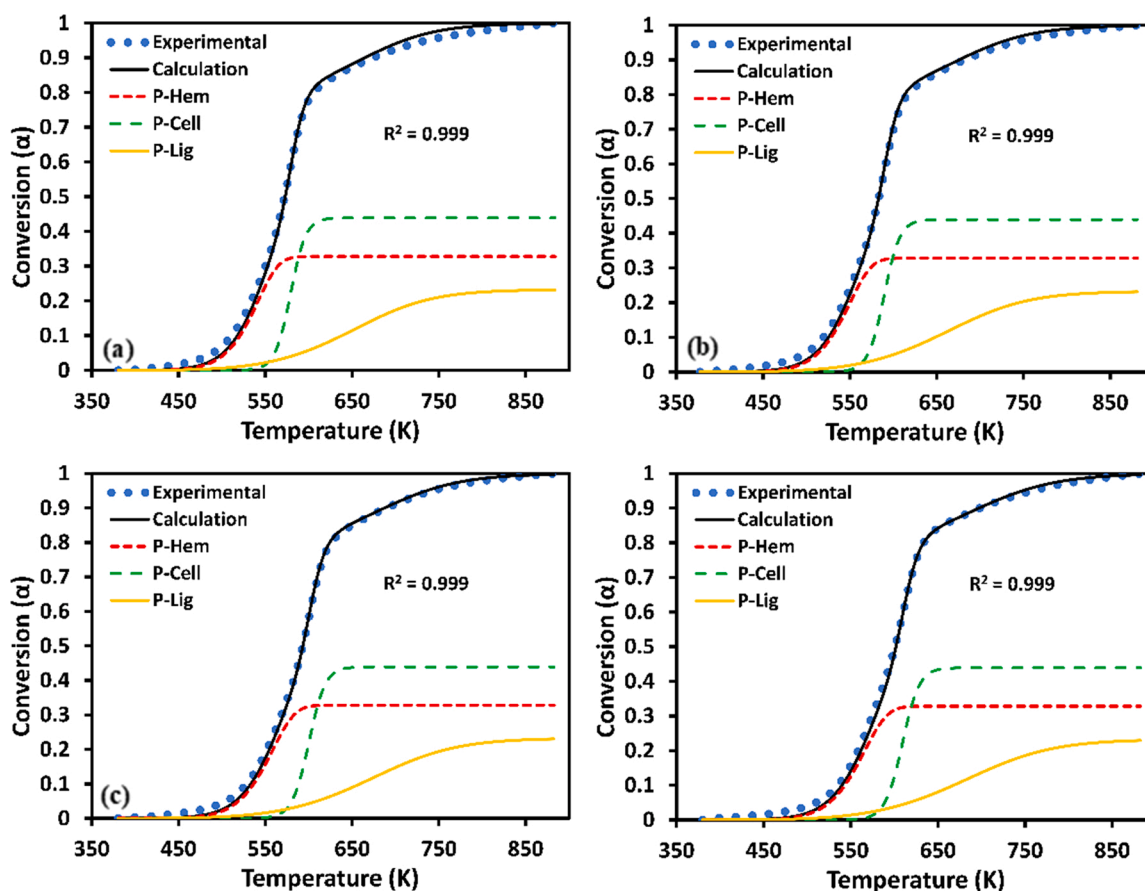


Fig. 12. TGA profiles comparison experimental and calculation CK of *Imperata Cylindrica* pyrolysis at four heating rates (a). 2.5 K/min, (b). 5 K/min, (c). 10 K/min, and (d). 17.5 K/min.

$$\frac{d\alpha_C}{dT} = \frac{4.246 \times 10^{15}}{\beta} \exp\left(\frac{-179968}{RT}\right) \alpha_C^{0.3313} (1 - \alpha_C)^{1.4731} [-\ln(1 - \alpha_C)]^{0.0215} \quad (2)$$

For P-Lig:

$$\frac{d\alpha_L}{dT} = \frac{4.524 \times 10^{15}}{\beta} \exp\left(\frac{-219226}{RT}\right) \alpha_L^{-2.9551} (1 - \alpha_L)^{2.7642} [-\ln(1 - \alpha_L)]^{0.0074} \quad (3)$$

As per ICTAC suggestion to verified the accuracy between calculation with experimental for all heating, the Eq. (1) to Eq. (3) could be arranged to estimate conversion rate $\left(\frac{d\alpha}{dT}\right)$ and conversion (α) for calculation data at four difference heating rates, as described in Eq. (4) dan Eq. (5).

$$\left(\frac{d\alpha}{dT}\right)_{\text{calculation}} = c_H \left(\frac{d\alpha_H}{dT}\right) + c_C \left(\frac{d\alpha_C}{dT}\right) + c_L \left(\frac{d\alpha_L}{dT}\right) \quad (4)$$

$$\alpha_{\text{calculation}} = c_H \cdot \alpha_H + c_C \cdot \alpha_C + c_L \cdot \alpha_L \quad (5)$$

Where c_H , c_C , and c_L were contribution factors and its values obtained from the Table 4 based on average of c_i value belong to respective pseudo components. The value of β is heating rate (K/min); R is the universal gas constant (8.314 J/mol.K); and T is temperature (K). The Eq. (1) to Eq. (3) would be solved by using 4th order Runge-Kutta method for respective heating rate. Figs. 11 (a–d) and 12 (a–d) show the results of the CK of IC pyrolysis at four heating rates. The results have been presented high coefficient correlation factors in the ranges $0.98 < R^2 < 0.999$ for TGA and DTG profiles of respective heating rates, which mean show that the CK describes the IC pyrolysis kinetic model fitted very well with experimental data for all heating rates.

5. Conclusion

A combination Asym2sig deconvolution and combined kinetics of the pyrolysis of IC was performed via thermogravimetric analysis (TGA) deconvolution, iso-conversional method, master plot analysis and combined kinetics. The kinetic study of pyrolysis process was performed following the multi step reaction, due to the heterogeneous pyrolysis process. Based on the results, reaction models of P-Hem, P-Cell and P-Lig were $f(\alpha) = \alpha^{-0.9875} (1 - \alpha)^{1.325} [-\ln(1 - \alpha)]^{0.0209}$, $f(\alpha) = \alpha^{0.3313} (1 - \alpha)^{1.4731} [-\ln(1 - \alpha)]^{0.0215}$ and $f(\alpha) = \alpha^{-2.9551} (1 - \alpha)^{2.7642} [-\ln(1 - \alpha)]^{0.0074}$, respectively. The value of $m = -0.9875$ for P-Hem and $m = -2.9951$ for P-Lig signify that there was contribution from the 2/3-Power law (P23) and 1-D diffusion (D1) model. The value $m = 0.3313$ for P-Cell denote caused by the power law (P2, P3 and P4) mechanism. The optimum parameters values of n were higher than 1st order model reaction for all pseudo components, which indicated that there are Geometrical contraction, Order based, and Diffusion model contribution. Through the combine kinetics the activation energies of the pseudo-components were reported as 194.709 kJ/mol, 179.968 kJ/mol and 219.226 kJ/mol for P-Hem, P-Cell and P-Lig, respectively. The value of E_{P-Cell} lower than the value of E_{P-Hem} and E_{P-Lig} , probably indicated the effect of structural heterogeneity, synergetic and the catalysing effects. Furthermore, the activation energy of P-Lig exhibited higher than P-Hem and P-Cell, indicated that lignin linkage ring of lignin was strong and caused a higher thermal stability than cellulose and hemicellulose. Therefore, the reaction rate of lignin was slow and occurred over the entire pyrolysis temperature interval.

CRedit authorship contribution statement

Syarif Hidayat: Conceptualization, Methodology, Formal analysis, Writing - original draft, Writing - review & editing. **Muhammad S. Abu Bakar:** Investigation, Supervision, Writing - original draft, Writing -

review & editing, Funding acquisition. **Ashfaq Ahmed:** Conceptualization, Methodology, Validation, Writing - original draft, Writing - review & editing. **Dewi Agustina Iryani:** Validation, Writing - original draft, Writing - review & editing. **Murid Hussain:** Validation, Writing - review & editing. **Farrukh Jamil:** Validation, Writing - review & editing. **Young-Kwon Park:** Supervision, Validation, Funding acquisition, Writing - review & editing.

Declaration of Competing Interest

The authors declare that they have no known competing financial interests or personal relationships that could have appeared to influence the work reported in this paper.

Acknowledgements

First author is grateful for the scholarship grant to the Ministry of Foreign Affairs and Trade (MOFAT), Brunei Darussalam and the support from the Integrated Laboratory and Technology Innovation Centre of University of Lampung. Also, the support from the Universitas Brunei Darussalam under the research grant (UBD/RSCH/1.3/FICBF(b)/2019/004) and National Research Foundation of Korea under the project (NRF- 2020R111A1A01072793, 2020M1A2A2079801) is gratefully acknowledged.

Appendix A. Supplementary data

Supplementary material related to this article can be found, in the online version, at doi:<https://doi.org/10.1016/j.jaap.2021.105133>.

References

- [1] S.H. Ansari, A. Ahmed, A. Razzaq, D. Hildebrandt, X. Liu, Y.-K.K. Park, Incorporation of solar-thermal energy into a gasification process to co-produce bio-fertilizer and power, *Environ. Pollut.* 266 (2020), <https://doi.org/10.1016/j.envpol.2020.115103>, 115103.
- [2] S.S. Moogi, J. Jae, H.P.R. Kannapu, A. Ahmed, E.D. Park, Y.K. Park, Enhancement of aromatics from catalytic pyrolysis of yellow poplar : role of hydrogen and methane decomposition, *Bioresour. Technol.* 315 (2020), <https://doi.org/10.1016/j.biortech.2020.123835>, 123835.
- [3] A. Farooq, S. Moogi, S.H. Jang, H.P.R. Kannapu, S. Valizadeh, A. Ahmed, S.S. Lam, Y.K. Park, Linear low-density polyethylene gasification over highly active Ni/CeO₂-ZrO₂ catalyst for enhanced hydrogen generation, *J. Ind. Eng. Chem.* 94 (2021) 336–342, <https://doi.org/10.1016/j.jiec.2020.11.005>.
- [4] A. Abdullah, A. Ahmed, P. Akhter, A. Razzaq, M. Zafar, M. Hussain, N. Shahzad, K. Majeed, S. Khurram, M.S.A. Bakar, Y.-K.K. Park, M. Saifullah, A. Bakar, Y.-K. K. Park, Bioenergy potential and thermochemical characterization of lignocellulosic biomass residues available in Pakistan, *Korean J. Chem. Eng.* 37 (2020) 1899–1906, <https://doi.org/10.1007/s11814-020-0624-0>.
- [5] P.K. Dikshit, H.B. Jun, B.S. Kim, Biological conversion of lignin and its derivatives to fuels and chemicals, *Korean J. Chem. Eng.* 37 (2020) 387–401, <https://doi.org/10.1007/s11814-019-0458-9>.
- [6] F. Jamil, M. Aslam, A.H. Al-Muhtaseb, A. Bokhari, S. Rafiq, Z. Khan, A. Inayat, A. Ahmed, S. Hossain, M.S. Khurram, M.S.A. Bakar, Greener and sustainable production of bioethylene from bioethanol: Current status, opportunities and perspectives, *Int. Rev. Chem. Eng.* 36 (2020), <https://doi.org/10.1515/revce-2019-0026>.
- [7] A. Ahmed, M.S. Abu Bakar, A.K. Azad, R.S. Sukri, T.M.I. Mahlia, Potential thermochemical conversion of bioenergy from Acacia species in Brunei Darussalam: a review, *Renew. Sustain. Energy Rev.* 82 (2017) 3060–3076, <https://doi.org/10.1016/j.rser.2017.10.032>.
- [8] A. Abdullah, A. Ahmed, P. Akhter, A. Razzaq, M. Hussain, N. Hossain, M.S. Abu Bakar, S. Khurram, K. Majeed, Y.K. Park, Potential for sustainable utilisation of agricultural residues for bioenergy production in Pakistan: An overview, *J. Clean. Prod.* (2020), <https://doi.org/10.1016/j.jclepro.2020.125047>, 125047.
- [9] A. Inayat, M. Inayat, M. Shahbaz, S.A. Sulaiman, M. Raza, S. Yusup, Parametric analysis and optimization for the catalytic air gasification of palm kernel shell using coal bottom ash as catalyst, *Renew. Energy* (2020), <https://doi.org/10.1016/j.renene.2019.06.104>.
- [10] G.E. MacDonald, Cogongrass (*Imperata cylindrica*)—biology, ecology, and management, *Crit. Rev. Plant Sci.* 23 (2004) 367–380, <https://doi.org/10.1080/07352680490505114>.
- [11] Y.K. Park, M.L. Yoo, S.H. Jin, S.H. Park, Catalytic fast pyrolysis of waste pepper stems over HZSM-5, *Renew. Energy* 79 (2015) 20–27, <https://doi.org/10.1016/j.renene.2014.10.005>.

- [12] S. Reza, A. Ahmed, W. Caesarendra, M.S.A. Bakar, S. Shams, R. Saidur, N. Aslfattahi, A.K. Azad, *Acacia Holosericea* : an invasive species for bio-char, bio-oil, and biogas production, *Bioengineering*. 6 (2019) 1–16, <https://doi.org/10.3390/bioengineering620033>.
- [13] A. Ahmed, M.S.M.S. Abu Bakar, R.S.R.S. Sukri, M. Hussain, A. Farooq, S. Moogi, Y.-K.Y.-K. Park, Sawdust pyrolysis from the furniture industry in an auger pyrolysis reactor system for biochar and bio-oil production, *Energy Convers. Manage.* 42 (2020), <https://doi.org/10.1016/j.enconman.2020.113502>, 556–549.
- [14] M.S. Abu Bakar, A. Ahmed, D.M. Jeffery, S. Hidayat, R.S. Sukri, T.M.I. Mahlia, F. Jamil, M.S. Khurram, A. Inayat, S. Moogi, Y.K. Park, Pyrolysis of solid waste residues from Lemon Myrtle essential oils extraction for bio-oil production, *Bioresour. Technol.* (2020) 1–5, <https://doi.org/10.1016/j.biortech.2020.123913>.
- [15] X. Zhang, H. Deng, X. Hou, R. Qiu, Z. Chen, Pyrolytic behavior and kinetic of wood sawdust at isothermal and non-isothermal conditions, *Renew. Energy* 142 (2019) 284–294, <https://doi.org/10.1016/j.renene.2019.04.115>.
- [16] D. Neves, H. Thunman, A. Matos, L. Tarelho, A. Gómez-Barea, Characterization and prediction of biomass pyrolysis products, *Prog. Energy Combust. Sci.* 37 (2011) 611–630, <https://doi.org/10.1016/j.peccs.2011.01.001>.
- [17] S. Vyazovkin, A.K. Burnham, J.M. Criado, L.A. Pérez-Maqueda, C. Popescu, N. Sbirrazzuoli, ICTAC Kinetics committee recommendations for performing kinetic computations on thermal analysis data, *Thermochim. Acta* 520 (2011) 1–19, <https://doi.org/10.1016/j.tca.2011.03.034>.
- [18] C. Gai, Y. Dong, T. Zhang, The kinetic analysis of the pyrolysis of agricultural residue under non-isothermal conditions, *Bioresour. Technol.* 127 (2013) 298–305, <https://doi.org/10.1016/j.biortech.2012.09.089>.
- [19] O. Oladokun, A. Ahmada, T.A. Tuan, Model free kinetics analysis of *imperata cylindrica* (Lalang), *J. Teknol.* 78 (2016) 25–31.
- [20] O. Oladokun, A. Ahmad, T.A.T. Abdullah, B.B. Nyakuma, A.A.H. Bello, A.H. Al-Shatri, Multicomponent devolatilization kinetics and thermal conversion of *Imperata cylindrica*, *Appl. Therm. Eng.* 105 (2016) 931–940, <https://doi.org/10.1016/j.applthermaleng.2016.04.165>.
- [21] P. Sharma, O.P. Pandey, P.K. Diwan, Non-isothermal kinetics of pseudo-components of waste biomass, *Fuel*. 253 (2019) 1149–1161, <https://doi.org/10.1016/j.fuel.2019.05.093>.
- [22] A. Anca-Couce, Reaction mechanisms and multi-scale modelling of lignocellulosic biomass pyrolysis, *Prog. Energy Combust. Sci.* 53 (2016) 41–79, <https://doi.org/10.1016/j.peccs.2015.10.002>.
- [23] J.C.G. da Silva, J.G. de Albuquerque, W.V. de A. Galdino, R.F. de Sena, S.L. F. Andersen, Single-step and multi-step thermokinetic study – Deconvolution method as a simple pathway for describe properly the biomass pyrolysis for energy conversion, *Energy Convers. Manage.* 209 (2020), <https://doi.org/10.1016/j.enconman.2020.112653>, 112653.
- [24] S. Vyazovkin, A.K. Burnham, L. Favregeon, N. Koga, E. Moukhina, L.A. Pérez-Maqueda, N. Sbirrazzuoli, ICTAC kinetics committee recommendations for analysis of multi-step kinetics, *Thermochim. Acta* 689 (2020), <https://doi.org/10.1016/j.tca.2020.178597>, 178597.
- [25] Z. Chen, M. Hu, X. Zhu, D. Guo, S. Liu, Z. Hu, B. Xiao, J. Wang, M. Laghari, Characteristics and kinetic study on pyrolysis of five lignocellulosic biomass via thermogravimetric analysis, *Bioresour. Technol.* 192 (2015) 441–450, <https://doi.org/10.1016/j.biortech.2015.05.062>.
- [26] A.O. Aboyade, M. Carrier, E.L. Meyer, J.H. Knoetze, J.F. Görgens, Model fitting kinetic analysis and characterisation of the devolatilization of coal blends with corn and sugarcane residues, *Thermochim. Acta* 530 (2012) 95–106, <https://doi.org/10.1016/j.tca.2011.12.007>.
- [27] M. Poletto, A.J. Zattera, R.M.C. Santana, Thermal decomposition of wood: kinetics and degradation mechanisms, *Bioresour. Technol.* 126 (2012) 7–12, <https://doi.org/10.1016/j.biortech.2012.08.133>.
- [28] Y. Ba, F. Liu, X. Wang, J. Yang, Pyrolysis of C3 energy plant (arundo donax): Thermogravimetry, mechanism, and potential evaluation, *Ind. Crops Prod.* 149 (2020), <https://doi.org/10.1016/j.indcrop.2020.112337>, 112337.
- [29] S. Naya, R. Cao, I.L. de Ullibarri, R. Arriaga, F. Barbadillo, A. García, Logistic mixture model versus Arrhenius for kinetic study of material degradation by dynamic thermogravimetric analysis, *J. Chemom.* 20 (2006) 158–163, <https://doi.org/10.1002/cem.1023>.
- [30] L.M. Romero Millán, F.E. Sierra Vargas, A. Nzihou, Kinetic analysis of tropical Lignocellulosic Agrowaste Pyrolysis, *Bioenergy Res.* 10 (2017) 832–845, <https://doi.org/10.1007/s12155-017-9844-5>.
- [31] A. Perejón, P.E. Sánchez-Jiménez, J.M. Criado, L.A. Pérez-Maqueda, Kinetic analysis of complex solid-state reactions. A new deconvolution procedure, *J. Phys. Chem. B* 115 (2011) 1780–1791, <https://doi.org/10.1021/jp110895z>.
- [32] C. Chen, W. Miao, C. Zhou, H. Wu, Thermogravimetric Pyrolysis Kinetics of Bamboo Waste Via Asymmetric Double Sigmoidal (Asym2sig) Function Deconvolution, 2016, <https://doi.org/10.1016/j.biortech.2016.11.013>.
- [33] G. Davi Mumbach, J. Luiz, F. Alves, J.C. Gomes, D. Silva, R. Felix De Sena, C. Marangoni, R. Antonio, F. Machado, A. Bolzan, Thermal investigation of plastic solid waste pyrolysis via the deconvolution technique using the asymmetric double sigmoidal function: Determination of the kinetic triplet, thermodynamic parameters. Thermal Lifetime and Pyrolytic Oil Composition for Clean, 2019, <https://doi.org/10.1016/j.enconman.2019.112031>.
- [34] J.L.F. Alves, J.C.G. Da Silva, M. Di Domenico, W.V.D.A. Galdino, S.L.F. Andersen, R.F. Alves, R.F. De Sena, Exploring açai seed (*Euterpe oleracea*) pyrolysis using multi-component kinetics and Thermodynamics assessment towards its bioenergy potential, *Bioenergy Res.* (2020) 1–17, <https://doi.org/10.1007/s12155-020-10175-y>.
- [35] S. Hidayat, M.S. Abu Bakar, Y. Yang, N. Phusunti, A.V. Bridgwater, Characterisation and Py-GC/MS analysis of *Imperata Cylindrica* as potential biomass for bio-oil production in Brunei Darussalam, *J. Anal. Appl. Pyrolysis* 134 (2018) 510–519, <https://doi.org/10.1016/j.jaap.2018.07.018>.
- [36] S. Vyazovkin, K. Chrissafis, M.L. Di Lorenzo, N. Koga, M. Pijolat, B. Roduit, N. Sbirrazzuoli, J.J. Suñol, ICTAC Kinetics Committee recommendations for collecting experimental thermal analysis data for kinetic computations, *Thermochim. Acta* 590 (2014) 1–23, <https://doi.org/10.1016/J.TCA.2014.05.036>.
- [37] A. Ahmed, M.S. Abu Bakar, A.K. Azad, R.S. Sukri, N. Phusunti, Intermediate pyrolysis of *Acacia cincinnata* and *Acacia holosericea* species for bio-oil and biochar production, *Energy Convers. Manage.* 176 (2018) 393–408, <https://doi.org/10.1016/j.enconman.2018.09.041>.
- [38] A.I. Osman, Mass spectrometry study of lignocellulosic biomass combustion and pyrolysis with NOx removal, *Renew. Energy* 146 (2020) 484–496, <https://doi.org/10.1016/j.renene.2019.06.155>.
- [39] A. Ahmed, S. Hidayat, M.S. Abu Bakar, A.K. Azad, R.S. Sukri, N. Phusunti, Thermochemical characterisation of *Acacia auriculiformis* tree parts via proximate, ultimate, TGA, DTG, calorific value and FTIR spectroscopy analysis to evaluate their potential as a biofuel resource, *Biofuels* 7269 (2018) 1–12, <https://doi.org/10.1080/17597269.2018.1442663>.
- [40] N. Radenahmad, N.A. Morni, A. Ahmed, M.Abu Bakar, J. Zaini, A. Azad, Characterization of rice husk as a potential renewable energy source, 7th Brunei Int. Conf. Eng. Technol. (BICET 2018) (2018) 1–4, <https://doi.org/10.1049/cp.2018.1527>.
- [41] H. Hassan, J.K. Lim, B.H. Hameed, Catalytic co-pyrolysis of sugarcane bagasse and waste high-density polyethylene over faujasite-type zeolite, *Bioresour. Technol.* 284 (2019) 406–414, <https://doi.org/10.1016/J.BIORTECH.2019.03.137>.
- [42] C. Huang, L. Han, Z. Yang, X. Liu, Ultimate analysis and heating value prediction of straw by near infrared spectroscopy, *Waste Manag.* 29 (2009) 1793–1797, <https://doi.org/10.1016/j.wasman.2008.11.027>.
- [43] J. Grams, M. Kwapińska, M. Jędrzejczyk, I. Rzeźnicka, J.J. Leahy, A.M. Ruppert, Surface characterization of *Miscanthus × giganteus* and Willow subjected to torrefaction, *J. Anal. Appl. Pyrolysis* 138 (2019) 231–241, <https://doi.org/10.1016/j.jaap.2018.12.028>.
- [44] S. Kanwal, N. Chaudhry, S. Munir, H. Sana, Effect of torrefaction conditions on the physicochemical characterization of agricultural waste (sugarcane bagasse), *Waste Manag.* 88 (2019) 280–290, <https://doi.org/10.1016/j.wasman.2019.03.053>.
- [45] J. Coates, Interpretation of infrared spectra, a practical approach. *Encycl. Anal. Chem.*, John Wiley & Sons, Ltd, 2006, <https://doi.org/10.1002/9780470027318.a5606>.
- [46] Y. Disco, P. Mahanta, U. Bora, Comprehensive characterization of lignocellulosic biomass through proximate, ultimate and compositional analysis for bioenergy production, *Renew. Energy* 103 (2017) 490–500, <https://doi.org/10.1016/j.renene.2016.11.039>.
- [47] A.E. Pütün, A. Özean, E. Pütün, Pyrolysis of hazelnut shells in a fixed-bed tubular reactor: Yields and structural analysis of bio-oil, *J. Anal. Appl. Pyrolysis* 52 (1999) 33–49, [https://doi.org/10.1016/S0165-2370\(99\)00044-3](https://doi.org/10.1016/S0165-2370(99)00044-3).
- [48] J. Park, J. Meng, K.H. Lim, O.J. Rojas, S. Park, Transformation of lignocellulosic biomass during torrefaction, *J. Anal. Appl. Pyrolysis* 100 (2013) 199–206, <https://doi.org/10.1016/j.jaap.2012.12.024>.
- [49] S. Nanda, P. Mohanty, K.K. Pant, S. Naik, J.A. Kozinski, A.K. Dalai, Characterization of North American Lignocellulosic Biomass and Biochars in Terms of their Candidacy for Alternate Renewable Fuels, *Bioenergy Res.* 6 (2013) 663–677, <https://doi.org/10.1007/s12155-012-9281-4>.
- [50] A. Anca-Couce, A. Berger, N. Zobel, How to determine consistent biomass pyrolysis kinetics in a parallel reaction scheme, *Fuel*. 123 (2014) 230–240, <https://doi.org/10.1016/j.fuel.2014.01.014>.
- [51] X. Wang, M. Hu, W. Hu, Z. Chen, S. Liu, Z. Hu, B. Xiao, Thermogravimetric Kinetic Study of Agricultural Residue Biomass Pyrolysis Based on Combined Kinetics, 2016, <https://doi.org/10.1016/j.biortech.2016.07.136>.
- [52] B.J. Janković, Kinetic analysis of the nonisothermal decomposition of potassium tetrakisulfite using the model-fitting and isoconversional (model-free) methods, *Chem. Eng. J.* 139 (2008) 128–135, <https://doi.org/10.1016/j.cej.2007.07.085>.
- [53] S. Pinzi, C. Buratti, P. Bartocci, G. Marseglia, F. Fantozzi, M. Barbanera, A simplified method for kinetic modeling of coffee silver skin pyrolysis by coupling pseudo-components peaks deconvolution analysis and model free-isoconversional methods, *Fuel*. (2020), <https://doi.org/10.1016/j.fuel.2020.118260>.
- [54] J.Y. Yeo, B.L.F. Chin, J.K. Tan, Y.S. Loh, Comparative studies on the pyrolysis of cellulose, hemicellulose, and lignin based on combined kinetics, *J. Energy Inst.* 92 (2019) 27–37, <https://doi.org/10.1016/J.JOEL.2017.12.003>.
- [55] S. Subramanian, U.B.R. Ragula, Kinetics of catalytic and non-catalytic pyrolysis of Nerium Oleander, *Fuel*. (2020), <https://doi.org/10.1016/j.fuel.2020.118591>.
- [56] H. Siddiqi, U. Kumari, S. Biswas, A. Mishra, B.C. Meikap, A synergistic study of reaction kinetics and heat transfer with multi-component modelling approach for the pyrolysis of biomass waste, *Energy*. 204 (2020), <https://doi.org/10.1016/j.energy.2020.117933>, 117933.
- [57] K. Dussan, S. Dooley, R. Monaghan, Integrating compositional features in model compounds for a kinetic mechanism of hemicellulose pyrolysis, *Chem. Eng. J.* (2017), <https://doi.org/10.1016/j.cej.2017.07.089>.
- [58] R. Moriana, Y. Zhang, P. Mischnick, J. Li, M. Ek, Thermal degradation behavior and kinetic analysis of spruce glucomannan and its methylated derivatives, *Carbohydr. Polym.* (2014), <https://doi.org/10.1016/j.carbpol.2014.01.086>.
- [59] J.B. Dahiya, K. Kumar, M. Muller-Hagedorn, H. Bockhorn, Kinetics of isothermal and non-isothermal degradation of cellulose: model-based and model-free methods, *Polym. Int.* (2008), <https://doi.org/10.1002/pi.2398>.
- [60] L. Abdelouahed, S. Leveneur, L. Vernieres-Hassimi, L. Balland, B. Taouk, Comparative investigation for the determination of kinetic parameters for biomass

- pyrolysis by thermogravimetric analysis, *J. Therm. Anal. Calorim.* (2017), <https://doi.org/10.1007/s10973-017-6212-9>.
- [61] X. Xd, X.X. Wang, X.X. Dai, X. Yang, X. Luo, Lignocellulosic Biomass Pyrolysis Mechanism: a State-of-the-art Review, 2017, <https://doi.org/10.1016/j.pecs.2017.05.004>.
- [62] C. Chio, M. Sain, W. Qin, Lignin Utilization: a Review of Lignin Depolymerization From Various Aspects, 2019, <https://doi.org/10.1016/j.rser.2019.03.008>.
- [63] A. Ozyuguran, A. Akturk, S. Yaman, Optimal use of condensed parameters of ultimate analysis to predict the calorific value of biomass, *Fuel*. 214 (2018) 640–646, <https://doi.org/10.1016/J.FUEL.2017.10.082>.